Journal of Hazardous Materials 185 (2011) 1053–1058

Contents lists available at ScienceDirect

Journal of Hazardous Materials

journal homepage: www.elsevier.com/locate/jhazmat

Deactivation mechanism of PtOx/TiO_2 photocatalyst towards the oxidation of NO in gas phase

Zhongbiao Wu[a,b], Zhongyi Sheng[a,b], Yue Liu[a,b,*], Haiqiang Wang[a,b], Jiansong Mo[b]

[a] Department of Environmental Engineering, Zhejiang University, Hangzhou 310027, PR China
[b] Zhejiang Provincial Engineering Research Center of Industrial Boiler & Furnace Flue Gas Pollution Control, Hangzhou 310027, PR China

ARTICLE INFO

Article history:
Received 25 May 2010
Received in revised form
25 September 2010
Accepted 4 October 2010
Available online 3 November 2010

Keywords:
TiO_2
PtOx
FTIR
NO adsorption
Photocatalysis

ABSTRACT

This study has been undertaken to investigate the roles of PtO and PtO_2 deposits in photocatalytic oxidation of NO over Pt-modified TiO_2 catalysts. These photocatalysts were prepared by neutralization method and characterized by XRD, BET, XPS, TEM and FTIR. It was found that Pt dopant existed as PtO and PtO_2 particles in as-prepared photocatalysts. And these Pt dopants would change their oxidation states during the photocatalytic oxidation reaction. An in situ XPS study indicated that a portion of PtO_2 on the surface of Pt/TiO_2 was reduced to PtO under UV irradiation. The migration of electrons to PtO_2 particles could separate the electrons and holes, resulting in the improvement of photocatalytic activity. And the depletion of PtO_2 by electrons could lead to the deactivation of Pt/TiO_2 catalyst. Moreover, PtO particles could be corroded to form Pt^{2+} ions by HNO_3, which was one of the products of photocatalytic oxidation of NO. NO would adsorb on Pt^{2+} related sites to form Pt^{n+}–NO nitrosyls, retarding photocatalytic oxidation of NO to NO_2.

1. Introduction

Nitrogen oxides (NOx) emissions to atmosphere have direct impact on the global environment and human health through ozone depletion, photochemical smog and the acid deposition [1,2]. Wet scrubbing method promises to an efficient and economical way to remove soluble pollutants [3]. In order to remove NOx by wet scrubbing method, it is necessary to oxidize nitric oxide (NO) to more soluble nitrogen dioxide (NO_2) or dinitrogen pentoxide (N_2O_5) in either gas or liquid phase [4,5]. However, it is very difficult to oxidize dilute NO except the addition of strong oxidants such as methanol, ozone and hydrogen peroxide [5–7].

The photocatalytic oxidation using titanium dioxide (TiO_2) as photocatalyst has been shown to be a relatively cheap and effective process to convert NO to NO_2 in gas phase [8–10]. When subjected to irradiation of wavelength less than 380 nm, a valence band electron is excited to the conduction band, generating an electron-hole pair that can recombine or initiate redox reactions [11,12]. The recombination probability between photogenerated electrons and holes is a major factor limiting the photocatalytic activity. Holes are trapped by water (H_2O) or hydroxyl groups (OH^-) adsorbed on the surface to generate hydroxyl radicals ($OH^\bullet$). Electrons reduce adsorbed oxygen (O_2) to yield superoxide ions ($O_2^{\bullet-}$). $OH^\bullet$ and $O_2^{\bullet-}$ groups are the main oxidants for NO oxidation [13]. It is reported that there are three states during photocatalytic oxidation process of NO [14–16]. At the initial state, the oxidation product is nitrous acid (HNO_2). And then in the transient state, oxidation of HNO_2 to NO_2 and subsequent oxidation of NO_2 to nitric acid (HNO_3) occur. Once the catalyst is saturated with HNO_3, the steady state reaches and the oxidation reaction can only go as far as NO_2. The nitrogen mass balance about NO and NO_2 is established at the steady state.

Our recent study has found that platinum oxides (PtOx) modified TiO_2 (Degussa P25) can improve effectively the photocatalytic oxidation activity of NO, while metallic platinum (Pt^0) and chloroplatinic ions ($PtCl_6^{2-}$) deposits on TiO_2 do not facilitate the photocatalytic activity [17]. Actually, PtOx could exist as PtO(II) and PtO_2(IV) particles on TiO_2 surface. However, the roles of PtO and PtO_2 dopants on photocatalytic oxidation of NO are still uncertain. Meanwhile, the deactivation mechanism of PtOx/TiO_2 was not clear. As an extension work of our previous study, we try to find out the roles of the PtO and PtO_2 dopants on photocatalytic oxidation of NO through investigating the photocatalytic behaviors. The method for modification of TiO_2 with PtOx is neutralization method. And the catalysts were characterized by X-ray diffraction analysis (XRD), Brunauer–Emmett–Teller measurements (BET), X-ray photoelectron spectrum analysis (XPS), transmission electron microscopy (TEM) and high-resolution-transmission electron microscopy (HR-TEM). Finally, the deactivation mechanism of

* Corresponding author at: Department of Environmental Engineering, Zhejiang University, Hangzhou 310027, PR China. Tel.: +86 571 87953088; fax: +86 571 87953088.
E-mail address: yueliu@zju.edu.cn (Y. Liu).

0304-3894/$ – see front matter © 2010 Elsevier B.V. All rights reserved.
doi:10.1016/j.jhazmat.2010.10.013

PtOx-modified TiO_2 towards photocatalytic oxidation of NO in gas phase was discussed.

2. Experimental

2.1. Catalysts preparation

Commercial TiO_2 Degussa P25 was used as the precursor. Chloroplatinic acid ($H_2PtCl_6{\cdot}6H_2O$) and sodium hydroxide (NaOH) were analytical grade. PtOx-modified TiO_2 (Pt/TiO_2) was prepared by neutralization method. The samples were prepared by dispersal of 8.0 g TiO_2 powder into 100 ml $H_2PtCl_6{\cdot}6H_2O$ solution (4–40 mg/100 ml) to obtain Pt loading of 0.05–0.5 wt.%. The pH value of the slurry was adjusted to pH 7 with 10% NaOH. Then the resulting suspension was aged at room temperature for 6 h. After aging, the samples were filtered, washed and dried at 100 °C. Then the samples were calcined at 400 °C for 2 h in air.

2.2. Catalysts characterization

XRD patterns were obtained by a Rigaku D/Max RA diffractometer with Cu Kα radiation at 40 kV and 150 mA, at an angle of 2θ from 20° to 80°. The size of the crystallites was calculated with the Scherrer equation [18]. The phase composition of the samples was estimated with the following equation [19]: $F_R = 1/\{1 + 0.79 [I_A\ (1\,0\,1)/I_R\ (1\,1\,0)]\}$. Here F_R is the mass fraction of rutile in the samples, and I_A (1 0 1) and I_R (1 1 0) are the integrated 1 0 1 intensities of anatase and 1 1 0 of rutile, respectively. BET surface areas (S_{BET}) were determined using N_2 physisorption at 77 K, with a Micromeritics ASSP 2020 equipment. Surface element analysis was carried out by XPS using a Thermo ESCALAB 250 instrument with Al Kα radiation ($h\nu$ = 1486.6 eV) at 150 W. The signal of adventitious carbon (a binding energy of 284.8 eV) has been used to calibrate the binding energy scale for XPS measurements. The morphology, structure and grain size of Pt/TiO_2 were examined by TEM and HR-TEM with a JEM-2010 instrument. In situ diffuse reflectance infrared transform (DRIFT) spectroscopy were acquired with Nicolet 6700 Fourier transform infrared (FTIR) spectrometer at 4 cm^{-1} resolution with 64 co-added scans. In DRIFT cell, the catalysts were pretreated at 150 °C in He environment for 2 h, then cooled to room temperature. The background spectra were recorded in flowing He and were subtracted from the sample spectra.

2.3. Photocatalytic activity measurements

The method of photocatalyst immobilization was carried out by the dip-coating method [15]. The experiment setup and operating conditions for photocatalytic activity tests were the same as that in our previous reports [20,21]. All the photocatalytic activity experiments were carried out in a continuous setup. The setup consisted of a gas supply, reactor and analytical system. An air compressor, a NO gas cylinder (10,000 ppm, diluted by N_2) and a N_2 gas cylinder (99.9%) were supplied as gas sources. By varying the flow rate of one stream air bubbled through a gas wash bottle, the humidity could be adjusted. The air, NO, and N_2 streams were mixed to obtain the desired concentration (NO: 100 ppm, relative humidity: 75%). The flow rate of the gas was 2.0 L/min and the residence time was 10 s. Photocatalytic experiments were carried out in a 340 ml cylindrical Pyrex glass reactor. The immobilized catalyst was set into the reactor with a "Z" type. The irradiation source was an Hg-arc lamp (125 W, Philips) located outside the reactor. The wavelength of the Hg-arc lamp varied in the range from 300 to 400 nm with the maximum light intensity at 365 nm. NO and NO_2 were analyzed with a NOx analyzer (Thermo Scientific, Model 42i-HL NO–NO_2–NOx Analyzer High Level). The relative humidity was measured with a relative humidity analyzer (Testo Co. Ltd., Model 605-H1).

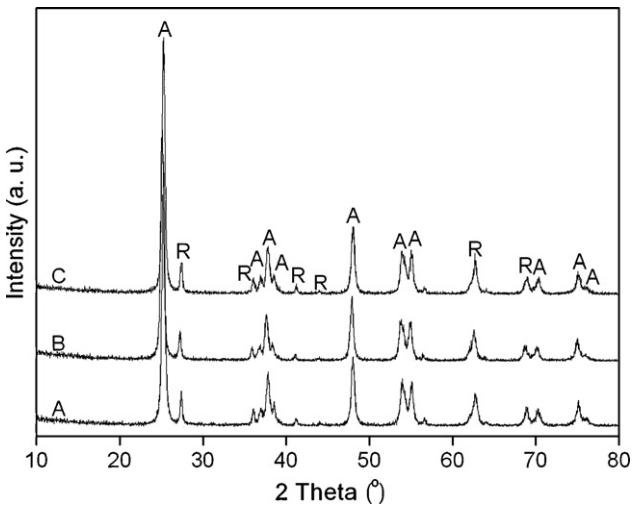

Fig. 1. XRD patters of catalysts with P25 (A) and different Pt dopant content of 0.05 wt.% (B), 0.5 wt.% (C).

Blank tests were conducted with the Hg-arc turned on but without the photocatalyst using 100 ppm inlet NO. The variation of the NO concentration couldn't be observed within 120 min irradiation. Furthermore, there was no change of the NO concentration when the Hg-arc lamp was turned off and the catalyst was present in the reactor.

3. Results and discussion

3.1. Characterization of Pt/TiO_2

The XRD patterns of P25 and Pt/TiO_2 photocatalysts are shown in Fig. 1. Peaks marked "A" and "R" correspond to anatase and rutile phases, respectively. The modification of Pt little changed the physical and morphological properties of the TiO_2, as listed in Table 1. Minor reductions in the specific area were found after Pt addition. These changes could be explained by the fact that the size of the crystallites of anatase and rutile increased on Pt-modified TiO_2. Furthermore, a small increment in the anatase fraction was also observed on Pt/TiO_2. These results indicated that there was little crystal transformation and crystal growth occurring in Pt modifying procedures. From the XRD patterns, all photocatalysts displayed a mixture of anatase and rutile, and no Pt-related compounds were detected, which indicated that Pt was loaded in the state of undetectably small particles.

The element composition was determined by XPS high-resolution scans over C 1s, O 1s, Cl 2p, Ti 2P and Pt 4f spectra regions. The atomic ratio of Pt on the surface of Pt/TiO_2 is shown in Table 1. Fig. 2 shows the Pt 4f peaks of 0.5 wt.% Pt/TiO_2 photocatalyst. The Pt $4f_{7/2}$ peak consisted of two individual peaks, corresponding to PtO and PtO_2. The peak at 72.2 eV can be attributed to PtO, and the peak at 74.05 was peculiar to PtO_2 [22–25]. The fraction of PtO on the surface was about 79.3% in the as-prepared sample. Vorontsov et al. [26] reported that different Pt deposits formed during the photocatalytic deposition and the Pt $4f_{7/2}$ binding energy of Pt metal, $Pt(OH)_2$, PtO_2 and $PtCl_6^{2-}$ was 70.5, 72.4–73.2, 73.3–74.1 and 75.2–75.6 respectively. In this study, the peak at 72.2 eV was considered as PtO instead of $Pt(OH)_2$, owing to the calcination process of the catalysts preparation.

The morphology of Pt/TiO_2 powders was further investigated by TEM images as shown in Fig. 3. The diameter of TiO_2 particles (Degussa P25) ranged from 20 to 50 nm, consistent with the value of the crystallite size determined by XRD spectra. From the HR-TEM image illustrated in Fig. 3b, it was confirmed that PtOx

Table 1
Physical and morphological properties of the photocatalysts.

Catalyst	S_{BET} (m^2/g)	Pt atomic concentration[a] (%)	Diameter[b] of TiO_2 (nm)	Rutile fraction[c] (%)
P25	52.3	–	20.3 (A); 30.3 (R)	10.06
0.05 wt.% Pt/TiO_2	49.4	0.078	21.0 (A); 29.5 (R)	9.58
0.5 wt.% Pt/TiO_2	48.7	0.59	21.2 (A); 30.8 (R)	8.87

[a] Pt atomic concentration is determined by XPS for the surface content of Pt on the Pt/TiO_2 photocatalysts.
[b] (A) stands for anatase and (R) for rutile.
[c] Rutile fraction means the fractions of rutile in TiO_2 (rutile and anatase).

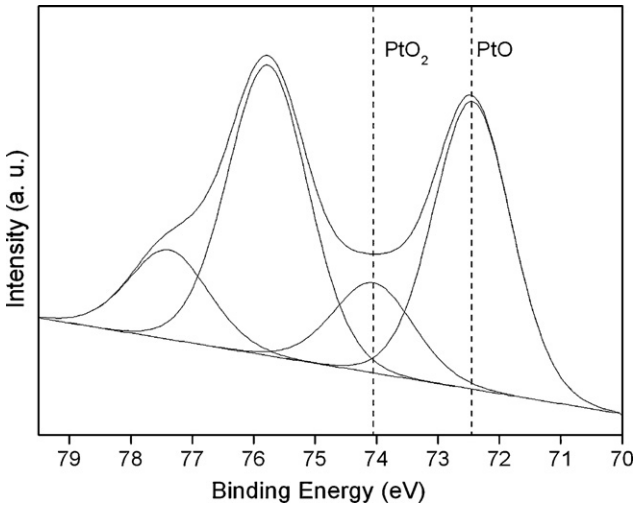

Fig. 2. XPS high-resolution scan over Pt 4f peaks on 0.5 wt.% Pt/TiO_2 photocatalyst.

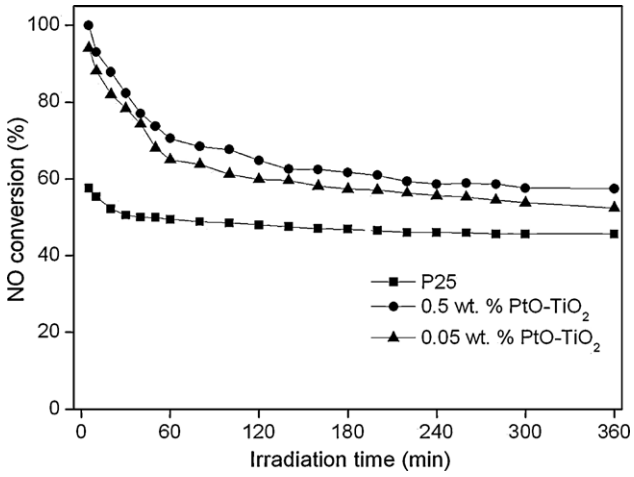

Fig. 4. Variations of NO conversion efficiency with irradiation time for P25, 0.05 wt.% Pt/TiO_2 and 0.5 wt.% Pt/TiO_2. Operating conditions: 125 W Hg-arc, 75% RH, 10 s residence time, 21% O_2 concentration and 100 ppm initial NO concentration.

particles were deposited on the surface of TiO_2, and their diameter predominantly ranged from 1 to 3 nm. However, it seemed difficult to determine from Fig. 3 whether PtO and PtO_2 constituted with a separate state in different particles or formed in a mixed state in the same particles.

3.2. Behaviors of photocatalytic oxidation

In the oxidation of NO over the studied photocatalysts, small amounts of HNO_2 and HNO_3 are produced at the initial and transient states of the reaction. NO_2 was the main product detected when the reaction approached the steady state. The NO conversion efficiency is estimated according to:

$$\text{NO conversion} = \frac{NO_{in} - NO_{out}}{NO_{in}} 100\% \quad (1)$$

where NO_{in} and NO_{out} are the inlet and outlet NO concentrations of photocatalytic reactor, respectively.

Fig. 4 shows the variations of NO conversion with irradiation time over P25 and Pt/TiO_2 catalysts under conditions of 75% relative humidity. The results obtained with P25 were displayed for comparison. A high conversion of NO (57.5%) was observed initially over P25. Then, the NO conversion decreased and approached a steady state (45.6%) after around 300 min of irradiation. Similar results could be found in literatures [14,15]. The curves in Fig. 4 reveal an evident difference in the performance of Pt/TiO_2. For 0.5 wt.% Pt/TiO_2 catalyst, the maximum conversion (100%) was observed at the beginning of reaction. And after 360 min of irradiation, the conversion decreased to 57.4%, which was only 25.9% higher than that with P25. And, it was also found that the main product of photocatalytic oxidation of NO was NO_2. Pt/TiO_2 catalyst showed a superior photocatalyst activity during the whole reaction process. However, the NO conversion decreased with irradiation time without a steady sate, which indicated that the deactivation process occurred in Pt/TiO_2 photocatalyst. These results indicated that the deposits of

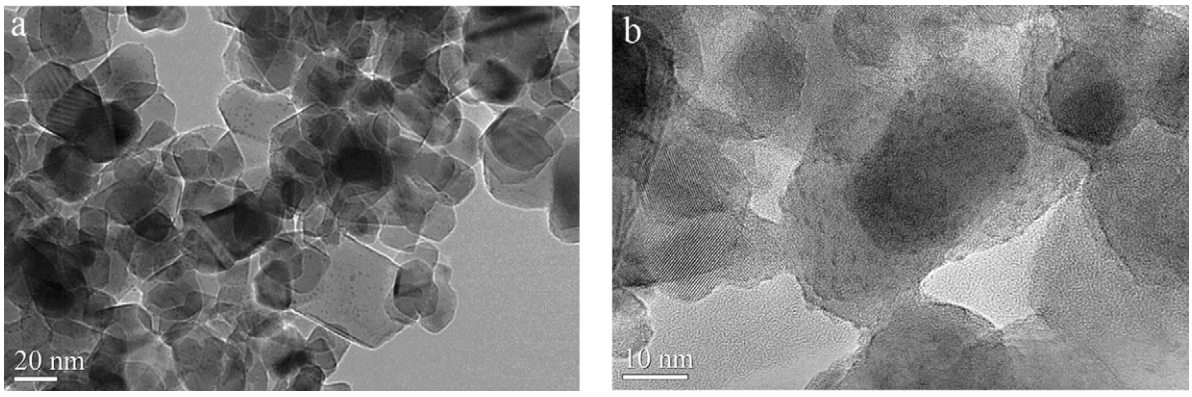

Fig. 3. TEM (a) and HR-TEM (b) images of 0.05 wt.% Pt/TiO_2.

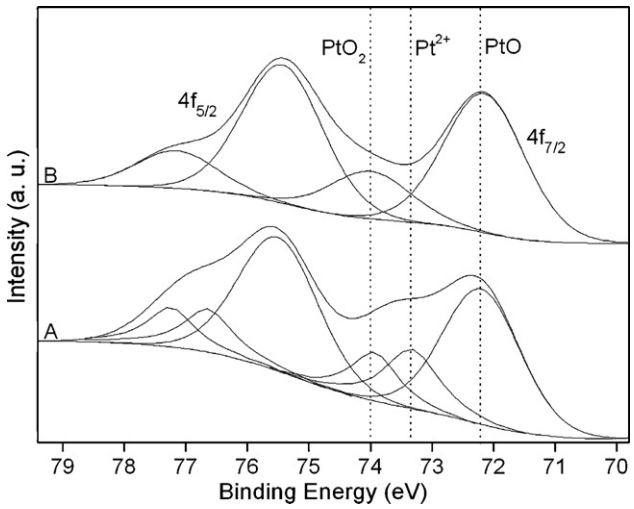

Fig. 5. XPS high-resolution scan over Pt 4f peaks on used 0.5 wt.% Pt/TiO_2 photocatalyst (A), and after regeneration (B).

Pt played key roles in the beneficial effect of photocatalytic activity and disadvantageous effect of catalyst durability.

Fig. 5A shows the XPS scan over Pt 4f peaks over 0.5 wt.% Pt/TiO_2 samples that was deactivated after photocatalytic oxidation of NO. From this figure, it could be seen that Pt 4f peaks were broadened in contrast to that before photocatalytic reaction (Fig. 2). The broad Pt $4f_{7/2}$ was well fitted as a combination of PtO (peak at 72.2 eV), Pt^{2+} (peak at 73.4 eV) and PtO_2 (peak at 74 eV). The fractions of PtO, Pt^{2+} and PtO_2 were about 63.7%, 20.9% and 15.4% in the deactivated sample, as shown in Table 2. In contrast to the sample before photocatalytic reaction (see Fig. 2 and Table 2), it is indicated that the fractions of PtO and PtO_2 both declined, and Pt^{2+} ions was formed during the photocatalytic oxidation process.

The regeneration test of deactivated PtOx-modified TiO_2 photocatalysts was also conducted to investigate the changes in the oxidation states of Pt under the deactivation and regeneration process. As shown in Fig. 6, the oxidation efficiency declined with the irradiation time, and the activity of catalyst recovered after the heat treatment at 400 °C. Similar results were reported in previous literatures [17]. Fig. 5B shows the XPS scan over Pt 4f peaks on 0.5 wt.% Pt/TiO_2 samples that was regenerated by calcination for 1 h. From Table 2, it could be seen that the fractions of PtO and PtO_2 increased, which suggested that Pt^{2+} ions on the deactivated catalyst was transferred to PtO and PtO_2 particles during the heat treatment process. The fraction of PtO_2 on regenerated sample was higher than that on fresh sample, leading to the higher activity after regeneration.

3.3. Deactivation mechanisms of Pt/TiO_2 catalyst

For Pt/TiO_2, the changes in the oxidation sates of Pt have been observed in the XPS scans over used samples as shown in Fig. 5, which could result in the deactivation of Pt/TiO_2 [20,21,27].

Table 2
Results of curve fitting of high-resolution XPS spectra for the Pt $4f_{7/2}$ peaks of 0.5 wt.% Pt/TiO_2 with fresh sample, deactivated sample and regenerated sample.

Sample	Pt $4f_{7/2}$ (atomic fraction[a], %)		
	PtO	Pt^{2+}	PtO_2
Fresh sample	79.3	–	20.7
Deactivated sample	63.7	20.9	15.4
Regenerated sample	75.1	–	24.9

[a] Atomic fraction means the fractions of PtO, Pt^{2+}, or PtO_2 in the total Pt element on the surface of Pt/TiO_2.

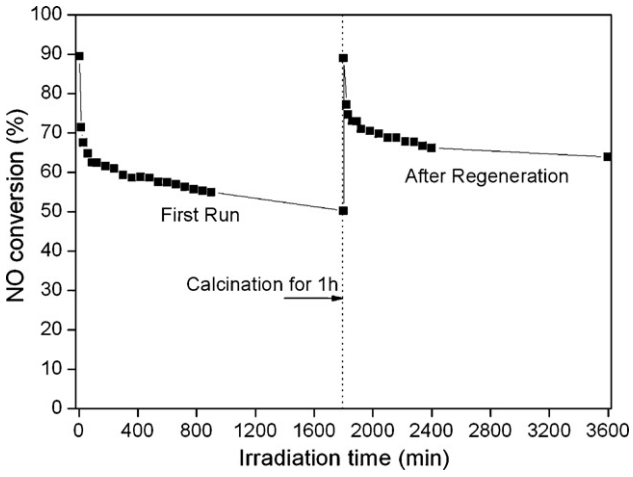

Fig. 6. The deactivation and regeneration test of 0.5 wt.% PtOx–TiO_2 with 60 h irradiation time. Operating conditions: 125 W Hg-arc, 75% RH, 10 s residence time, 21% O_2 concentration and 100 ppm initial NO concentration.

3.3.1. Effect of UV irradiation

To investigate the changes in the valence state of Pt on TiO_2 under UV irradiation, an in situ XPS study was conducted. 0.5 wt.% Pt/TiO_2 was first placed in the dark under the ultrahigh vacuum condition of XPS system overnight to make absorbed H_2O on the surface desorbed before XPS scans. Then, these samples were irradiated by UV light. XPS scans were performed after 0.5 and 3 h irradiation. Fig. 7 shows the Pt 4f peaks of Pt/TiO_2 in the dark, after 0.5 and 3 h irradiation, respectively. The fractions of PtO and PtO_2 on the surface were about 61.7% and 38.3% in the dark. After 3 h irradiation, the fractions of PtO and PtO_2 changed to 69.9% and 30.1%, which clearly suggested that a portion of PtO_2 on the surface of Pt/TiO_2 was reduced to PtO under the UV irradiation. When irradiated by UV light with wavelength less than 380 nm, electron–hole pairs on TiO_2 were generated [11,12]. PtO_2 particles dispersed on TiO_2 surface were populated with the generated electrons, leading to the transformation of PtO_2 to PtO (see Eq. (2)). And $O^{\bullet -}$ groups could be oxidized to oxygen molecules by holes, as shown in Eq. (3) [28].

$$PtO_2 + e_{CB}^- \rightarrow PtO + O^{\bullet -} \quad (2)$$

$$2O^{\bullet -} + 2h_{VB}^+ \rightarrow O_2 \quad (3)$$

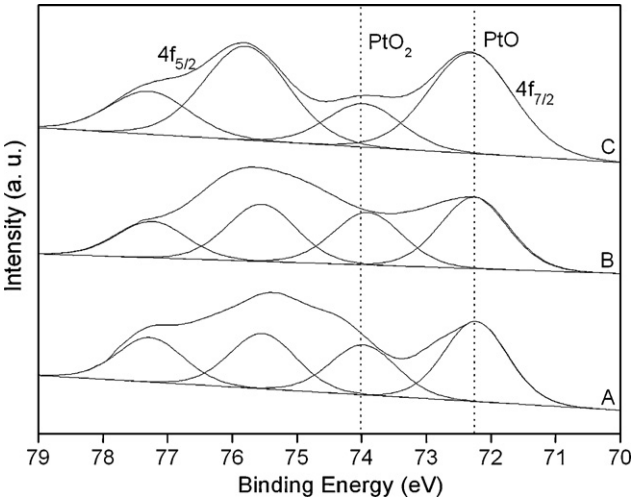

Fig. 7. Comparison of XPS high-resolution scans over Pt 4f peaks on 0.5 wt.% Pt/TiO_2 in the dark (A), after 0.5 (B) and 3 h (C) irradiation. UV irradiation source: He I ($h\nu$ = 21.2 eV), vacuum: $2–3 \times 10^{-7}$ Pa.

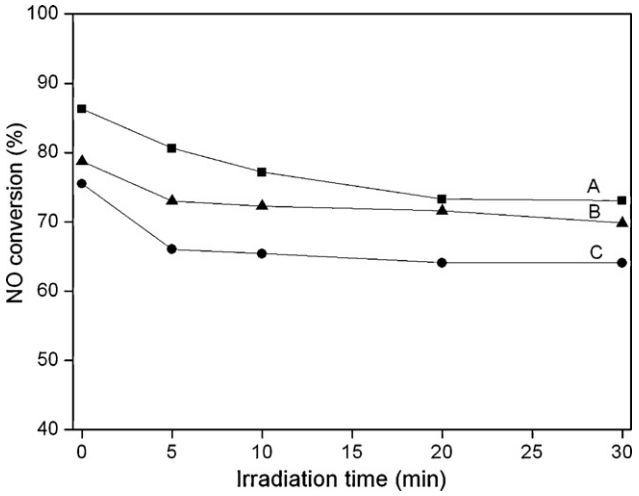

Fig. 8. Comparison of the conversion of NO with irradiation time over fresh sample (A), the sample treated with UV irradiation for 3 h (B) and the sample treated with HNO_3 by 3 h (C). Operating conditions: 125 W Hg-arc, 75% RH, 10 s residence time, 21% O_2 concentration and 100 ppm initial NO concentration.

For the photocatalytic oxidation of NO over Pt/TiO_2, photogenerated electrons were transferred from TiO_2 conduction band to the PtO_2 particles and a portion of PtO_2 particles would be reduced to PtO (see Eq. (2)). When the photogenerated electrons migrated to PtO_2, electrons and holes were efficiently separated, leading to the improvement of photocatalytic activity. With the depletion of PtO_2 particles, the conversion of NO decreased. Fig. 8 shows the comparison of the conversion of NO with irradiation time over fresh sample (A), the sample treated with UV irradiation for 3 h (B) and the sample treated with HNO_3 by 3 h (C). The catalyst was set into the reactor, and then turned on the UV light. The stream flowed through the reactor without NO. After 3 h, the NO stream was blended into the stream and the activity test started. As shown in Fig. 8, the conversion over the samples irradiated by UV light for 3 h was 12% lower than fresh sample. This test was directly indicated that the PtO_2 particles on TiO_2 provided a key contribution to the improvement of photocatalytic activity, while PtO deposits had no positive effect or played only a small part in NO oxidation.

3.3.2. *Effect of HNO_3*

Previous work has reported that HNO_3, HNO_2 and NO_2 were the products of NO oxidation [14,15]. It could be assumed that Pt^{2+} ions on the catalyst surface were formed through the following routes:

$$PtO_2 + 2H^+ \rightarrow Pt^{2+} + H_2O_2 \quad (4)$$

Table 3
Assignments of FTIR bands observed upon adsorption of NO on used 0.5 wt.% Pt/TiO_2.

Wavenumbers (cm^{-1})	Assignment	References
1326	Adsorbed nitro compounds, $\nu(-NO_2)$	[36]
1461	Almost symmetric stretching mode of bidentate nitrate, $\nu(NO_3)$	[31]
1508	Monodentate nitrate, $\nu(NO_3)$	[31,33]
1645	Pt^0–NO nitrosyls	[37]
1697	A weakly held form of adsorbed NO on Pt	[38]
1743	Pt^{n+}–NO species	[36]

Fig. 8C shows the photocatalytic activity of Pt/TiO_2 sample treated by HNO_3. The catalyst was set into the reactor. A stream including HNO_3 vapor was blended into the reactor. After 3 h, the photocatalytic activity test started. As shown in Fig. 8, the conversion was 5% lower than fresh sample. To investigate the effect of Pt^{2+} on TiO_2, an in situ FTIR study was conducted to investigate the NO adsorption over fresh and used photocatalysts.

In situ DRIFT spectra of the fresh and used Pt/TiO_2 during exposure to NO/He at room temperature are shown in Fig. 9. The spectra covering the range 900–1800 cm^{-1} were recorded to elucidate the chemical structure of NOx species adsorbed on 0.5 wt.% Pt/TiO_2 before and after photocatalytic oxidation. Bands at 1027, 1257, 1296, 1481, 1538, 1583, 1612 and 1650 cm^{-1} were detected on fresh Pt/TiO_2, as shown in Fig. 9a. The adsorption bands observed can be attributed to bidentate and monodentate nitrates [13,29–34]. The formation of surface nitrates on TiO_2 could be proposed as the following reactions (see Eqs. (5) and (6)) [32].

$$3NO + OH^- \rightarrow NO_2 + NO^- + NOH \quad (5)$$

$$3NO_2 + 2OH^- \rightarrow 2NO_3^- + NO + H_2O \quad (6)$$

On used Pt/TiO_2 catalyst, the bands at 1326, 1461, 1508, 1583, 1612, 1645, 1697 and 1743 cm^{-1} were detected, as shown in Fig. 9b. Bands at 1583 and 1612 cm^{-1} were weaker than on fresh catalyst. The new bands at 1326 cm^{-1} due to adsorbed nitro compounds, and at 1645, 1697 and 1743 cm^{-1} due to Pt-related species appeared. Table 3 summaries the assignment of all bands on the used photocatalyst except those observed in Fig. 9a. Ivanova et al. [35] proposed that adsorption of NO on Pt would form Pt^0–NO and Pt^{n+}–NO nitrosyls. Hadjiivanov [36] reported that the frequency of Pt^{n+}–NO mononitrosyls was above at 1710 cm^{-1} and these species were stable. Here, it is considered that the Pt-related species were formed by the adsorption of NO on Pt^{2+} ions.

XPS study over used sample indicated that a portion of PtO particles were corroded by HNO_3 to form Pt^{2+} ions (see Eq. (4)). The

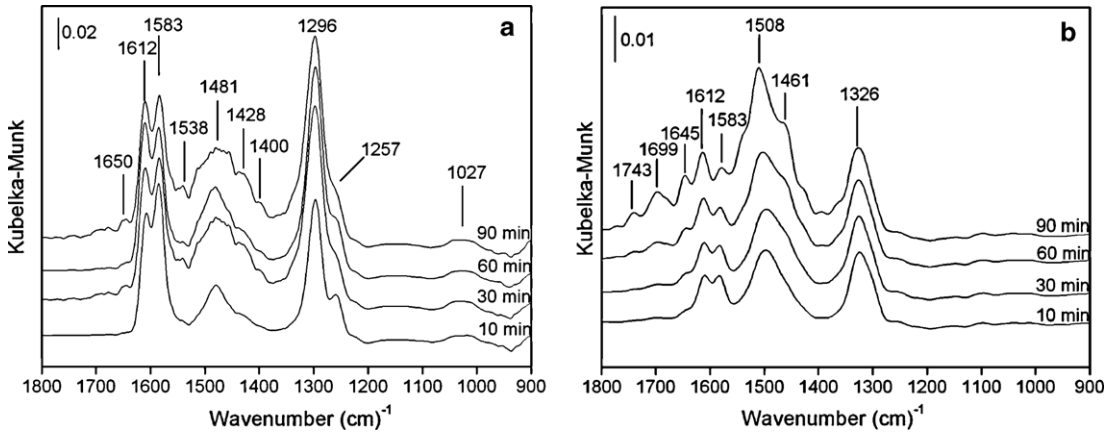

Fig. 9. In situ DRIFT spectra of fresh (a) and used (b) 0.5 wt.% Pt/TiO_2 during exposure to 400 ppm NO (balanced by He) at room temperature for 10, 30, 60 and 90 min.

adsorption sites of NO were different on the used photocatalysts, resulting in the formation of nitro compounds, Pt^0–NO nitrosyls, and Pt^{n+}–NO mononitrosyls. When irradiated by UV lights, $OH^\bullet$ and $O_2^{\bullet-}$ groups preferentially oxidized nitrosyls to form nitro compounds, thereby deferring the oxidation of NO [13]. With the consumption of $OH^\bullet$ and $O_2^{\bullet-}$ groups, the photocatalytic activity decreased. A proposed mechanism for the adsorption of NO on used Pt/TiO_2 and the formation of nitro compounds by photocatalytic oxidation is shown as the following route.

$$Pt^{n+} + NO \xrightarrow{\text{adsorption on } TiO_2} Pt^{n+} - NO \text{ Nitrosyls}$$

$$\xrightarrow{OH\cdot \text{and } O_2^{\bullet-} \text{ groups}} \text{Nitro compounds} \quad (7)$$

4. Conclusions

In this study, PtOx-modified TiO_2 photocatalysts were prepared by neutralization method and used for the photocatalytic oxidization of NO. The experimental results showed that the effective oxidation state of Pt on TiO_2 surface was PtO_2. PtO_2 particles deposited on TiO_2 could accept the photogenerated electrons to form PtO, and then electrons and holes were efficiently separated, leading to the improvement of photocatalytic activity. With the depletion of PtO_2, the conversion declined gradually. Furthermore, the corrosion of PtO to form Pt^{2+} by HNO_3 could change the adsorption sites of NO on TiO_2 surface. Pt^{n+}–NO nitrosyls could retard photocatalytic oxidation of NO to NO_2, resulting in another possible reason for the deactivation of Pt/TiO_2 photocatalysts.

Acknowledgments

This work was financially supported by the National High-Tech Research and Development Program (863) of China (2007AA061701), the National Natural Science Foundation of China (50908201), and Changjiang Scholar Incentive Program, Ministry of Education, PR China (2009).

References

[1] A. Farrell, Multi-lateral emission trading: lessons from inter-state NOx control in the United States, Energy Policy 29 (2001) 1061–1072.
[2] T. Castro, S. Madronich, S. Rivale, A. Muhlia, B. Mar, The influence of aerosols on photochemical smog in Mexico City, Atmos. Environ. 35 (2001) 1765–1772.
[3] J. Jeong, K. Sekiguchi, M. Saito, Y. Lee, Y. Kim, K. Sakamoto, Removal of gaseous pollutants with a UV-$C_{254+185}$ nm/TiO_2 irradiation system coupled with an air washer, Chem. Eng. J. 118 (2006) 127–130.
[4] Y.G. Adewuyi, S.O. Owusu, Aqueous absorption and oxidation of nitric oxide with oxone for the treatment of tail gases: process feasibility, stoichiometry, reaction pathways, and absorption rate, Ind. Eng. Chem. Res. 42 (2003) 4084–4100.
[5] Y.S. Mok, Absorption-reduction technique assisted by ozone injection and sodium sulfide for NOx removal from exhaust gas, Chem. Eng. J. 118 (2006) 63–67.
[6] J.M. Haywood, C.D. Cooper, The economic feasibility of using hydrogen peroxide for the enhanced oxidation and removal of nitrogen oxides from coal-fired power plant flue gases, J. Air Waste Manage. Assoc. 48 (1998) 238–246.
[7] V.M. Zamansky, L. Ho, P.M. Maly, W.R. Seeker, Oxidation of NO to NO_2 by hydrogen peroxide and its mixtures with methanol in natural gas and coal combustion gases, Combust. Sci. Technol. 120 (1996) 255–272.
[8] T. Ibusuki, K. Takeuchi, Removal of low concentration of nitrogen oxides through photoassisted heterogeneous catalysis, J. Mol. Catal. 88 (1994) 93–102.
[9] C.H. Ao, S.C. Lee, C.L. Mak, L.Y. Chan, Photodegradation of volatile organic compounds (VOCs) and NO for indoor air purification using TiO_2: promotion versus inhibition effect of NO, Appl. Catal. B 42 (2003) 119–129.
[10] C.H. Ao, S.C. Lee, Enhancement effect of TiO_2 immobilized on activated carbon filter for the photodegradation of pollutants at typical indoor air level, Appl. Catal. B 44 (2003) 191–205.
[11] A.L. Linsebigler, G.Q. Lu, J.T. Yates Jr., Photocatalysis on TiO_2 surfaces: principles, mechanisms, and selected results, Chem. Rev. 95 (1995) 735–758.
[12] M.R. Hoffmann, S.T. Martin, W. Choi, D.W. Bahnemann, Environmental applications of semiconductor photocatalysis, Chem. Rev. 95 (1995) 69–96.
[13] J.C.S. Wu, Y.T. Cheng, In situ FTIR study of photocatalytic NO reaction on photocatalysts under UV irradiation, J. Catal. 237 (2006) 393–404.
[14] S. Devahasdin, C. Fan Jr., K. Li, D.H. Chen, TiO_2 photocatalytic oxidation of nitric oxide: transient behavior and reaction kinetics, J. Photochem. Photobiol. A 156 (2003) 161–170.
[15] H.Q. Wang, Z.B. Wu, W.R. Zhao, B.H. Guan, Photocatalytic oxidation of nitrogen oxides using TiO_2 loading on woven glass fabric, Chemosphere 66 (2007) 185–190.
[16] Z.B. Wu, H.Q. Wang, Y. Liu, Z.L. Gu, Photocatalytic oxidation of nitric oxide with immobilized titanium dioxide films synthesized by hydrothermal method, J. Hazard. Mater. 151 (2008) 17–25.
[17] H.Q. Wang, Z.B. Wu, Y. Liu, Y.J. Wang, Influences of various Pt dopants over surface platinized TiO_2 on the photocatalytic oxidation of nitric oxide, Chemosphere 74 (2008) 773–778.
[18] M.C. Yan, F. Chen, J.L. Zhang, M. Anpo, Preparation of controllable crystalline titania and study on the photocatalytic properties, J. Phys. Chem. B 109 (2005) 8673–8678.
[19] M. Hirano, C. Nakahara, K. Ota, O. Tanaike, M. Inagaki, Photoactivity and phase stability of ZrO_2-doped anatase-type TiO_2 directly formed as nanometer-sized particles by hydrolysis under hydrothermal conditions, J. Solid State Chem. 170 (2003) 39–47.
[20] Z.Y. Sheng, Z.B. Wu, Y. Liu, H.Q. Wang, Gas-phase photocatalytic oxidation of NO over palladium modified TiO_2 catalysts, Catal. Commu. 9 (2008) 1941–1944.
[21] Z.B. Wu, Z.Y. Sheng, Y. Liu, H.Q. Wang, N. Tang, J. Wang, Characterization and activity of Pd-modified TiO_2 catalysts for photocatalytic oxidation of NO in gas phase, J. Hazard. Mater. 164 (2009) 542–548.
[22] J.C. Yang, Y.C. Kim, Y.G. Shul, C.H. Shin, T.K. Lee, Characterization of photoreduced Pt/TiO_2 and decomposition of dichloroacetic acid over photoreduced Pt/TiO_2 catalysts, Appl. Surf. Sci. 121–122 (1997) 525–529.
[23] K.C. Cho, K.C. Hwang, T. Sano, K. Takeuchi, S. Matsuzawa, Photocatalytic performance of Pt-loaded TiO_2 in the decomposition of gaseous ozone, J. Photochem. Photobiol. A 161 (2004) 155–161.
[24] V. Pitchon, A. Fritz, The relation between surface state and reactivity in the DeNOx mechanism on platinum-based catalysts, J. Catal. 186 (1999) 64–74.
[25] S. Yin, T. Sato, Photocatalytic activity of platinum loaded fibrous titania prepared by solvothermal process, J. Photochem. Photobiol. A 169 (2005) 89–94.
[26] A.V. Vorontsov, E.N. Savinov, Z.S. Jin, Influence of the form of photodeposited platinum on titania upon its photocatalytic activity in CO and acetone oxidation, J. Photochem. Photobiol. A 125 (1999) 113–117.
[27] Z.B. Wu, Z.Y. Sheng, H.Q. Wang, Y. Liu, Relationship between Pd oxidation states on TiO_2 and the photocatalytic oxidation behaviors of nitric oxide, Chemosphere 77 (2009) 264–268.
[28] A. Fujishima, T.N. Rao, D.A. Tryk, Titanium dioxide photocatalysis, J. Photochem. Photobiol. C 1 (2000) 1–21.
[29] I. Nakamura, S. Sugihara, K. Takeuchi, Mechanism for NO photooxidation over the oxygen-deficient TiO_2 powder under visible light irradiation, Chem. Lett. 11 (2000) 1276–1277.
[30] D.V. Pozdnyakov, V.N. Fillmonov, Use of irspectroscopy to investigate chemisorption of nitric oxide and nitrogen dioxide on metallic oxides, Kinet. Catal. 14 (1973) 655–660.
[31] G. Ramis, G. Busca, V. Lorenzelli, P. Rorzatti, Fourier transform infrared study of the adsorption and coadsorption of nitric oxide, nitrogen dioxide and ammonia on TiO_2 anatase, Appl. Catal. 64 (1990) 243–257.
[32] M. Kantcheva, Identification, stability, and reactivity of NOx species adsorbed on titania-supported manganese catalysts, J. Catal. 204 (2001) 479–494.
[33] K. Hadjiivanov, V. Bushev, M. Kantcheva, D. Klissurski, Infrared spectroscopy study of the species arising during nitrogen dioxide adsorption on titania (anatase), Langmuir 10 (1994) 464–471.
[34] M. Kantcheva, V. Bushev, K. Hadjiivanov, Nitrogen dioxide adsorption on deuteroxylated titania (anatase), J. Chem. Soc., Faraday Trans. 88 (1992) 3087–3089.
[35] E. Ivanova, M. Mihaylov, F. Thibault-Starzyk, M. Daturi, K. Hadjiivanov, FTIR spectroscopy study of CO and NO adsorption and co-adsorption on Pt/TiO_2, J. Mol. Catal. A 274 (2007) 179–184.
[36] K.I. Hadjiivanov, Identification of neutral and charged NxOy surface species by IR spectroscopy, Catal. Rev. 42 (2000) 71–144.
[37] C. Panja, B.E. Koel, Influence of alloyed Sn on adsorption and reaction of NO on Pt (1 0 0) surfaces, J. Phys. Chem. A 104 (2000) 2486–2497.
[38] B.A. Morrow, R.A. McFarlane, L.E. Moran, Infrared study of the reaction between nitric oxide and molecular oxygen and of the adsorption of nitrogen dioxide on platinum, J. Phys. Chem. 89 (1985) 77–80.